Southern Illinois University Carbondale
OpenSIUC

Articles | Department of Mechanical Engineering and Energy Processes

2016

Electrodeposition of MoS2 for Charge Storage in Electrochemical Supercapacitors

Daniel Falola
Southern Illinois University Carbondale

Tomasz Wiltowski
Southern Illinois University Carbondale, tomek@siu.edu

Ian Suni
Southern Illinois University Carbondale, isuni@siu.edu

Follow this and additional works at: http://opensiuc.lib.siu.edu/meep_articles

Recommended Citation

Falola, Daniel, Wiltowski, Tomasz and Suni, Ian. "Electrodeposition of MoS2 for Charge Storage in Electrochemical Supercapacitors." *Journal of the Electrochemical Society* 163, No. 9 (Jan 2016): D568-D574. doi:10.1149/2.0011610jes.

This Article is brought to you for free and open access by the Department of Mechanical Engineering and Energy Processes at OpenSIUC. It has been accepted for inclusion in Articles by an authorized administrator of OpenSIUC. For more information, please contact opensiuc@lib.siu.edu.

Electrodeposition of MoS_2 for Charge Storage in Electrochemical Supercapacitors

Bamidele D. Falola,[a,d] Tomasz Wiltowski,[c] and Ian I. Suni[,a,b,d]*

[a]Department of Mechanical Engineering and Energy Processes

[b]Department of Chemistry and Biochemistry

[c]Advanced Coal and Energy Research Center

[d]Materials Technology Center

Southern Illinois University

Carbondale, IL 62901

Abstract

Mo sulfide thin films were cathodically electrodeposited onto glassy carbon electrodes (GCE) from aqueous electrolytes containing 10 mM $(NH_4)_2MoS_4$ and 0.2 M KCl. Film adhesion was adequate only for electrodes pretreated by potential cycling in 1.0 M HNO_3 and 0.1 M NaF to enhance the surface roughness and partially oxidize the GCE. Previous studies report direct cathodic electrodeposition of MoS_2, but energy dispersive x-ray spectroscopy and x-ray diffraction suggest that the as-deposited film is closer in stoichiometry to MoS_3, which can be converted to MoS_2 by annealing in Ar at 600°C for one hour. The charge storage capability of electrodeposited Mo sulfide films is studied here for the first time in 1.0 M Na_2SO_4 over the thickness range 50 nm to 5 µm, and before and after high temperature annealing. The highest

21 capacitance is obtained for 50 nm thick MoS_2 films is 330 F/g measured by galvanostatic charge

22 discharge at 0.75 A/g, and 360 F/g measured by cyclic voltammetry at 10 mV/sec. The

23 capacitance per unit mass decreases with increasing film thickness due to reduced

24 electrochemical accessibility. MoS_2 film formed by high temperature annealing in Ar have a

25 charge storage capability about 40x higher than the as-deposited Mo sulfide films.

26

27 *Corresponding Author. Phone: 618-453-7922, E-mail address: isuni@siu.edu.

28

29

30

31 Molybdenum disulfide (MoS_2) is a layered transition metal sulfide that has been extensively
32 studied for applications such as catalysis,[1] solid phase lubrication,[2] two-dimensional transistors,[3]
33 electronic/spintronic devices,[4] materials for intercalation chemistry,[5] and electrodes for lithium ion
34 batteries.[6] The unique properties of MoS_2 arise from its two dimensional structure that is analogous to
35 that of graphene, with strong Mo-S covalent bonds formed within each layer, and weaker van der Waals
36 bonds between adjacent layers.[7,8] MoS_2 thin films have been fabricated predominantly by chemical vapor
37 deposition (CVD),[9,10] mechanical and chemical exfoliation,[11,12] hydrothermal synthesis,[13,14] microwave
38 heating,[15] and solution phase synthesis.[16,17] Cathodic MoS_2 electrodeposition has also been reported both
39 directly from MoS_4^{2-} precursors and from MoO_4^{2-} electrolytes that also contain either thiosulfate or sulfide
40 as the sulfur source.[18-22] Electrodeposition of MoS_2 is typically simpler and more cost-effective than
41 CVD and related methods, which involve complex and expensive vacuum technologies. In addition,
42 electrodeposition yields nm to µm thick films much more rapidly than exfoliation-based methods.
43 Compared to other solution phase methods, electrodeposition provides excellent control of film thickness.
44 Electrodeposition is widely studied for inexpensive scale-up of thin film applications such as photovoltaic
45 devices and electrochemical supercapacitors.[23] On the other hand, electrodeposition at low temperature
46 does not typically yield crystalline or polycrystalline deposits without post-processing.

47 In electrochemical supercapacitors, thin film metal oxides are often deposited atop high surface
48 area porous carbon electrodes,[24] which may contain activated carbon, carbon fiber-cloth, carbide-derived
49 carbon, carbon aerogel, graphite, graphene, or carbon nanotubes.[25] The metal oxide coating stores charge
50 during electrode polarization by valence change of the metal ion, thus contributing additional
51 pseudocapacitance to the electrostatic double layer capacitance at the electrode-electrolyte interface.[24]
52 For such applications, desirable properties include chemical stability and corrosion resistance, high
53 electrical conductivity, widespread abundance, non-toxicity, and high surface area per unit volume and
54 mass. The most intensively studied metal oxide coatings for supercapacitor applications include RuO_2,
55 MnO_2, and TiO_2.[26-30]

56 To date, metal sulfides have attracted less attention than metal oxides as pseudo-capacitive
57 electrode materials within electrochemical supercapacitors. However, chalcogenides such as MoS_2 are
58 intriguing for energy storage applications due to their layered structure, which allows for easier transport
59 and insertion of Li^+ within battery electrodes, as well as ion transport during oxidation and reduction of
60 metal oxide thin films.[7,8] However, while MoS_2 within electrochemical supercapacitors has recently been
61 widely studied, these studies have focused not on MoS_2 thin films, but on complex, composite structures
62 of nm to µm dimensions in order to optimize the total interfacial active area, and therefore maximize the
63 capacitance per unit mass.[7,8] Here we report cathodic electrodeposition of MoS_2 atop glassy carbon
64 electrodes, as well as detailed testing of MoS_2 thin film capacitance, both as a function of film thickness
65 and before and after high temperature annealing.

66

67 **Experimental**

68

69 Ammonium tetrathiomolybdate [$(NH_4)_2MoS_4$], KCl, and NaF were obtained from Acros
70 Organics. Anhydrous, ACS-grade Na_2SO_4 was obtained from Sigma Aldrich, while concentrated HNO_3
71 was purchased from Alfa Aesar. Glassy carbon electrodes (GCE) embedded within a Teflon sleeve were
72 purchased from CH Instruments, and glassy carbon plate was purchased from Alfa Aesar. All reagents
73 were used as received.

74 Prior to MoS_2 electrodeposition, the GCE was hand polished with 1.0, 0.3, and 0.05 µm alumina
75 powders. For most experiments, the GCE was subsequently given an electrochemical pretreatment of
76 potential cycling at room temperature between +1.5 and -0.4 V vs. Ag/AgCl at 50 mV/s for 300 cycles in
77 an electrolyte containing 1 M HNO_3 and 0.1 M NaF, and then rinsed with ultrapure water. This
78 procedure is a slight modification of a previously reported method for corrosion studies of glassy carbon
79 electrodes.[31] This electrochemical pretreatment process was employed here to enhance the surface
80 roughness and partially oxidize the GCE. This pre-treatment process significantly improves film-substrate

81 adhesion, since electrodeposited Mo sulfide films delaminated during capacitance measurements without
82 this pre-treatment.

83 Glassy carbon electrode (GCE) and glassy carbon plate, with and without MoS_2 coating, were
84 used as the working electrodes in a virgin Teflon three-electrode electrochemical cell with a Pt counter
85 electrode and an Ag/AgCl reference electrode. The GCE had an active area of 0.092 cm^2, while the
86 glassy carbon plate had an active area of 0.589 cm^2prior to annealing and 0.118 cm^2 after annealing.
87 Since the electrochemical cell had to be dissembled following Mo sulfide electrodeposition, and
88 subsequently reassembled following thin film annealing (described below), a smaller O-ring was
89 employed upon cell reassembly to ensure that only substrate regions with an electrodeposited thin film are
90 exposed to the electrolyte during subsequent studies. Cyclic voltammetry (CV), galvanostatic charge
91 discharge (GCD), and electrochemical impedance spectroscopy (EIS) measurements were performed with
92 a Gamry Instruments Reference 600. EIS measurements over the frequency range 0.01 Hz to 15 kHz
93 employ an AC probe amplitude of 5 mV, and each scan takes about 2.8 min. to acquire.

94 For some experiments, MoS_2 electrodeposits onto glassy carbon plate were subsequently
95 annealed in Ar at 600°C for 1 h in a Lindberg Blue M tube furnace. These deposits were then
96 analyzed by scanning electron microscopy (SEM) and energy dispersive x-ray spectroscopy (EDX) in a
97 Quanta 450 FEG from FEI Corp, atomic force microscopy in a Nanosurf FlexAFM, and by powder x-ray
98 diffraction (XRD) in a Rigaku MiniFlex II x-ray diffractometer. Film thickness measurements were
99 performed by stylus profilometery.

100

101 **Results and Discussion**

102

103 **Electrodeposition of Mo sulfide:** Figure 1 shows cyclic voltammetry (CV) results for a glassy
104 carbon electrode (GCE) in an electrolyte containing 10 mM $(NH_4)_2MoS_4$ and 0.2 M KCl at pH 6.8.
105 By comparison to a blank CV scan, the cathodic peak at approximately -1.0 V vs. Ag/AgCl

106 corresponds to electrodeposition of a Mo sulfide species. While the research group of Levy-
107 Clement first reported cathodic electrodeposition of MoS_2 from MoS_4^{2-},[18-20] they did not report
108 cathodic voltammetry peaks such as that observed in Figure 1. However, cathodic peaks varying
109 from about -400 to -600 mV vs. Ag/AgCl were reported for Mo sulfide electrodeposition during
110 successive voltage sweeps through both cathodic and anodic peaks for aqueous solutions
111 containing MoS_4^{2-} without a supporting electrolyte.[32] In addition, a cathodic peak was reported at
112 about -1.1 V vs. Ag/AgCl in weakly acidic electrolytes without attribution to a specific cathodic
113 reaction.[33] Electrochemical reduction of Mo sulfide from MoS_4^{2-}-containing electrolytes has
114 been attributed to the following reaction:[18-20]
115

116

$$MoS_4^{2-} + 4H^+ + 2e^- \rightarrow MoS_2 + 2H_2S \quad (1)$$

117

118 However, the results from subsequent annealing and EDX analysis of the MoS_2 thin films, combined with
119 powder x-ray diffraction (XRD), suggest that the species formed at the cathodic peak in Figure 1 is closer
120 in stoichiometry to MoS_3 than to MoS_2. On the other hand, since the precursor contains Mo(VI), the
121 cathodic reaction evident in Figure 1 probably cannot directly deposit MoS_3, which also contains Mo(VI).
122 It is possible that reaction (1) is correct, but subsequent chemical/electrochemical reactions result in
123 additional sulfur incorporation into the deposit.

124 Modest H_2 evolution is visually observed during cathodic electrodeposition of Mo sulfide.
125 Comparison of the film thickness measured by profilometery and the total charge transferred during
126 potentiostatic deposition suggests the current efficiency for electrodeposition of Mo sulfide is about 62%.
127 Potentiostatic electrodeposition at -1.0 V vs. Ag/AgCl allows growth of Mo sulfide films of varying
128 thickness. Mo sulfide films more than several μm thick contain nm scale cracks. Some Mo
129 sulfide films were grown on glassy carbon plate and subsequently annealed in Ar at 600°C for 1 h.
130 After this annealing process, cracks were no longer visible in thicker MoS_2 films.

131

132 **Thin Film Characterization:** Following the annealing treatment described above, Figure 2
133 illustrates top-view and cross-sectional SEM images of a MoS_2 thin film that is approximately 5 μm thick
134 atop a glassy carbon electrode. While such measurements are not fully quantitative, EDX results before
135 and after annealing are consistent with recrystallization of MoS_2 during this process. Prior to annealing,
136 the elemental composition varied, but the elemental Mo:S ratio was always close to 1:3. For annealed
137 films, EDX analyses consistently yield an elemental ratio of Mo:S equal to 1:2 to within experimental
138 error. Loss of sulfur during high temperature annealing is consistent with the low boiling point (444.6°C)
139 of elemental sulfur. AFM measurements over a 5x5 μm^2 scan range show that the high temperature
140 annealing process also reduces the rms surface roughness from 231 to 7 nm for a 5 μm thick film.
141 Powder x-ray diffraction (XRD) yields no peaks for the Mo sulfide film prior to high temperature
142 annealing. On the other hand, annealed Mo sulfide films yield the XRD pattern shown in Figure 3. This
143 exhibits a broad strong (002) peak at approximately 14.5°, consistent with the formation of crystalline
144 MoS_2.[34,35] From the (002) peak width in Figure 3, the grain size is estimated as 4.3 nm from the Scherrer
145 equation. However, higher peaks that could distinguish between the 2H and 3R polytypes are not
146 observed. Taken together, the EDX and XRD results suggest that the cathodic peak at -1.0 V does not
147 correspond directly to the reaction given in Equation 1, since stoichiometric MoS_2 is only formed after
148 high temperature annealing and loss of a significant amount of sulfur.
149

150 **Capacitance Testing:** As noted above, the research group of Levy-Clement previously reported
151 cathodic electrodeposition of MoS_2 from MoS_4^{2-},[18-20] but to the best of our knowledge, nobody has studied
152 the charge storage capability of electrodeposited MoS_2 thin films. The charge storage capability of Mo
153 sulfide thin films was assessed, before and after high temperature annealing, as a function of film
154 thickness by cyclic voltammetry and galvanostatic charge discharge measurements. During
155 measurements on glassy carbon electrodes (GCE) prepared by mechanical polishing only, the Mo sulfide
156 films delaminated quickly, resulting in a low capacitance value of about 500 $\mu F/cm^2$ after 100 scans.
157 Delamination occurs due to the poor adhesion between the Mo sulfide thin films and the GCE. Therefore

158 subsequent electrodeposition experiments were preceded by potential cycling between +1.5 and -0.4 V vs.
159 Ag/AgCl for 300 cycles at room temperature in an electrolyte containing 1 M HNO_3 and 0.1 M NaF in
160 order to electrochemically roughen and partially oxidize the surface of the GCE, as described above.

161 To demonstrate the potential applications of electrodeposited Mo sulfide thin films as
162 supercapacitor electrodes, its electrochemical performance was investigated by cyclic
163 voltammetry (CV) in 1.0 M Na_2SO_4 at pH 5.1. Figure 4 illustrates the CV curves for 1.0 µm
164 thick as-deposited MoS_3 and three thicknesses of annealed MoS_2 films at different scan rates
165 ranging from 5 to 100 mV/s over the potential range -200 to +400 mV vs. Ag/AgCl reference
166 electrode. The results in Figure 4 exhibit no cathodic or anodic current peaks, so the Mo sulfide
167 films studied here are close to ideal pseudocapacitive materials, albeit over a modest potential
168 window of ~600 mV.[36] From these cyclic voltammograms, the capacitance (C) per unit mass
169 (m) can be determined according to:

170

171 $$C = \frac{S}{2mk\left(U_2 - U_1\right)} \quad (2)$$

172

173 where S is the area enclosed by each curve, k is the scan rate, and U_2 - U_1 is the potential range scanned.
174 The capacitance per unit area (A) can also be obtained from Equation (2) by replacing mass with area.
175 Although studies of thin film metal capacitors often report the capacitance per unit mass, capacitance per
176 unit area is a more fundamental measure of charge storage capability. Such comparisons allow
177 quantitative determination of the value of extra MoS_2 film thickness for increasing the electrode
178 capacitance. One might expect thin film pseudo-capacitance to be limited to only a thin film region near
179 the electrode surface due to transport limitations for ion penetration into the bulk electrode material.

180 Comparing Figures 4a and 4c, the specific capacitance of the as-deposited MoS_3 is about 40x
181 lower than that of the annealed MoS_2 films, so further analysis was performed only on the latter. The low
182 capacitance of the as-deposited film is consistent with deposition of an amorphous film of non-

183 stoichiometric Mo sulfide. The improved film pseudocapacitance after annealing can be attributed to the
184 layered chalcogenide structure, where the relatively weak interlayer bonding provides mechanical
185 flexibility to accommodate ion transport during electrochemical reactions.[7,8]

186 Figure 5 summarizes the results for capacitance testing over 1000 cycles of MoS_2 films from 50
187 nm to 5 μm thick in 1.0 M Na_2SO_4 at a scan rate of 10 mV/sec. As the film thickness increases from 50
188 nm to 5 μm, the capacitance per unit mass in Figure 5 decreases continuously. This is consistent with
189 previous studies of transition metal oxide pseudocapacitance that suggest a penetration depth of 20-50 nm
190 for protons and other species involved in charge storage.[37-39] Material further below the solid-electrolyte
191 interface becomes electrochemically inaccessible, and this is thus at least partly inactive for charge
192 storage. This suggests that the best capacitance obtained here (350-400 F/g at 10 mV/sec) for 50 nm thick
193 MoS_2 cannot be increased much further by electrodeposition of thinner films. Figure 5 illustrates that
194 after 1000 cycles, 50 nm MoS_2 films retain 87% of their original capacitance, and films 250 nm and
195 thicker films retain 90-100% of their original capacitance. Figure 6 illustrates the effect of scan rate on
196 the measured capacitance for a range of MoS_2 film thickness. The decrease in film capacitance with
197 increasing scan rate is often observed for MoS_2 and other materials tested within electrochemical
198 supercapacitors,[40-42] and is expected for the current study due to the relatively thick (μm range) films
199 tested. However MoS_2 electrodes thicker than 50 nm demonstrate excellent capacitance performance at
200 high scan rate. For instance, the specific capacitance, as shown in Figure 6, of 125 nm thick MoS_2
201 electrode at scan rate of 100 mV/s is about 80% comparing with that at 10 mV/s, and this percentage
202 increases with film thickness.

203 MoS_2 film capacitance was also determined by galvanostatic charge discharge (GCD)
204 measurements, with Figure 7 illustrating the GCD results for three different MoS_2 film thickness: 50 nm,
205 1 μm, and 5 μm. The GCD curves are close to the triangular shape expected for ideal pseudocapacitive
206 behavior, except for the lowest current densities studied.[43,44] The capacitance can be precisely
207 determined from the GCD curves using the equation:[45]

208

209 $$C = \frac{i}{m\frac{dU}{dt}} \tag{3}$$

210

211 where i is the discharge current and dU/dt is the derivative of the discharge curve.

212 Figure 8 illustrates the effect of charge/discharge current density on the MoS_2 film capacitance
213 calculated from GCD measurements. The decline in film capacitance with increasing current density in
214 Figure 8 reflects the same underlying phenomena as the decline in capacitance with increasing scan rate
215 in Figure 6, reduced energy storage capability for high power applications. Similar to what is observed
216 for specific capacitance vs. scan rate in Figure 6, MoS_2 electrodes thicker than 50 nm demonstrate good
217 capacitance performance at high current density. Specifically, the specific capacitance of 125 nm thick
218 MoS_2 electrode at current density of 5 A/g is about 80% comparing with that at 1 A/ g. Figure 9
219 summarizes the capacitance measurements obtained for MoS_2 films of different thickness by
220 galvanostatic charge discharge. Figure 9 illustrates that capacitance retention ranges from 74-91% for the
221 different MoS_2 film thickness studied. The current densities at which each curve is given in Figure 9 are
222 chosen for a close correspondence to Figure 5a.

223 The highest capacitance per unit mass obtained for annealed MoS_2 is observed for 50 nm thick
224 films, and ranges from 350-400 F/g from both cyclic voltammetry at 10 mV/sec (Figure 5a) and
225 galvanostatic charge discharge at 0.75 A/g (Figure 9). These values can be compared to other reports of
226 MoS_2 incorporation into electrochemical supercapacitors, but often the materials tested do not correspond
227 to bulk MoS_2 films such as those electrodeposited here, so these comparison must be carefully made. For
228 example, many capacitance measurements on pure MoS_2 involves materials with only 1-3 monolayers
229 thick, whose electronic properties differ substantially from those of bulk MoS_2. In addition, many
230 researchers have studied composite materials that are not purely MoS_2, and their results depend on
231 composition, structure, grain size, and porosity, as well as scan or charging rate.

232 The authors are aware of only three studies of the capacitance of relatively thick, purely MoS_2
233 thin films.[40-42] Hydrothermal synthesis of porous MoS_2 thin films has been reported with capacitance up

234 to 403 F/g.[39] Magnetron sputtering has been employed to grow porous MoS_2 films of capacitance 330
235 F/cm^3.[41] In addition, MoS_2 and graphene nanofilms were grown separately by exfoliation, and then
236 combined into thin film geometry by co-precipitation, yielding film capacitance values as high as 13
237 mF/cm^2.[42] In summary, the best capacitance values obtained here (350-400 F/g) for 50 nm MoS_2 films
238 are similar to the results from references #40-42 for relatively thick MoS_2 films. Higher capacitance
239 values ranging from 416-589 F/g have been reported for MoS_2 nanocomposites with reduced graphene
240 oxide,[43] carbon nanotubes,[46] porous carbon,[47] polyaniline,[48] and WS_2 and amorphous carbon.[49] In
241 addition, much higher capacitance values up to 1544 F/g have been reported for MoS_2-Ni_2S_3
242 nanocomposites atop porous C and Ni electrodes.[50,51]

243 The nature and stability of annealed MoS_2 thin films of different thickness were further
244 investigated by electrochemical impedance spectroscopy (EIS) in 1.0 M Na_2SO_4. EIS studies are
245 sometimes employed to verify that materials intended for charge storage within electrochemical
246 supercapacitors are truly pseudocapacitive, and thus can be charged and discharged rapidly.[36] The results
247 for a 1.0 µm thick annealed MoS_2 film, before and after capacitance testing by cyclic voltammetry , are
248 shown in Figure 10. In these Nyquist plots, the real component of the impedance is plotted on the x-axis
249 and the imaginary component on the y-axis. For materials that undergo redox reactions, the Nyquist plot
250 exhibits a semicircular shape at intermediate to high frequencies, indicating relatively slow charge
251 transfer. The results in Figure 10 are consistent with truly pseudocapacitive materials, with the expected
252 capacitive behavior approaching a vertical line.[43] The results for other MoS_2 film thickness are almost
253 identical.

254 In addition, the results of Figure 10 suggest that the electrical properties of the MoS_2 thin film are
255 largely unaffected by capacitance testing. However, the slight reduction in the x-intercept likely indicates
256 that the MoS_2 film resistance decreases slightly during capacitance testing. Although the difference in the
257 x-intercepts is small, this is a real affect, since the electrochemical cell was not disturbed during these
258 measurements, so the electrode positions remain fixed.

259

260 **Conclusions**

261

262 Mo sulfide thin films can be cathodically electrodeposited onto glassy carbon from aqueous
263 electrolytes containing 10 mM $(NH_4)_2MoS_4$ and 0.2 M KCl at pH 6.8. EDX measurements yield a Mo:S
264 elemental ratio of about 1:3 in the as-deposited films, but this changes to 1:2 after annealing at 600°C in
265 Ar for one h. Similarly, the as-deposited Mo sulfide films do not exhibit any XRD peaks, but a broad
266 MoS_2 (002) peak is observed after high temperature annealing. From the Scherrer equation, the grain size
267 is estimated as 4.3 nm. For the first time, the charge storage capability of electrodeposited Mo sulfide
268 films is studied by potential scanning and galvanostatic charge discharge measurements in 1.0 M Na_2SO_4
269 over the thickness range 50 nm to 5 μm. The highest capacitance obtained ranges from 350-400 F/g for
270 50 nm thick MoS_2 films. MoS_2 film formed by high temperature annealing in Ar have a charge storage
271 capability about 40x higher than the as-deposited Mo sulfide films.

272

273

274 **References**

275

276 1. E.G. Firmiano, M.A. Cordeiro, A.C. Rabelo, C.J. Dalmaschio, A.N. Pinheiro, E.C. Pereira, and
277 R. Leite, *Chem. Commun*., **48**, 7687 (2012).
278 2. J.R. Lince, *Trib. Lett*., **17**, 419 (2004).
279 3. B. Radisavljevic, A. Radenovic, J. Brivio, V. Giacometti, and A. Kis, *Nat. Nanotech*., **6**, 147
280 (2011).
281 4. A. Dankert, L. Langouche, M.V. Kamalakar, and S.P. Dash, *ACS Nano*, **8**, 476 (2014).
282 5. E. Benavente, M. Santa Ana, F. Mendizábal, and G. González, G., *Coord. Chem. Rev*., **224**, 87
283 (2002).
284 6. K. Chang and W. Chen, *ACS Nano*, **5**, 4720 (2011).
285 7. X. Rui, H. Tan, and Q. Yan, *Nanoscale*, **6**, 9889 (2014).
286 8. M. Pumera, Z. Sofer, and A. Ambrosi, *J. Mater. Chem. A*, **2**, 8981 (2014).
287 9. A. Yan, J. Velasco, S. Kahn, K. Watanabe, T. Taniguchi, F. Wang, M.F. Crommie, and A. Zettl,
288 *Nano Lett*., **15**, 6324 (2015).
289 10. Y.H. Lee, X.Q. Zhang, W. Zhang, M.T. Chang, C.T. Lin, K.D. Chang, Y.C. Yu, J.T.W. Wang,
290 C.S. Chang, and L.J. Li, *Adv, Mater*., **24**, 2320 (2012).
291 11. K.G. Zhou, M.N. Mao, H.X. Wang, Y. Peng, and H.L. Zhang, *Angew. Chem. Inter. Ed*., **50**,
292 10839 (2011).
293 12. M.B. Sadan, L. Houben, A.N. Enyashin, G. Seifert, and R. Tenne, *Proc. Nat. Acad. Sci*., **105**,
294 15643 (2008).
295 13. X. Zhou, B. Xu, Z. Lin, D. Shu, and L. Ma, *J. Nanosci. Nanotechnol.*, **14**, 7250 (2014).
296 14. D. Kong, H. Wang, J.J. Cha, M. Pasta, K.J. Koski, J. Yao, and Y. Cui, *Nano Lett*., **13**, 1341
297 (2013).
298 15. E.G. da Silveira Firmiano, A.C. Rabelo, C.J. Dalmaschio, A.N. Pinheiro, E.C. Pereira, W.H.
299 Schreiner, and E.R. Leite, *Adv, Energy Mater*., **4**, 1301380 (2014).
300 16. C. Altavilla, M. Sarno, and P. Ciambelli, *Chem. Mater*., **23**, 3879 (2011).

301 17. K. Chang and W. Chen, *Chem. Commun*., **47**, 4252 (2011).
302 18. E.A. Ponomarev, M. Neumann-Spallart, G. Hodes, and C. Levy-Clement, *Thin Solid Films*, **280**,
303 86 (1996).
304 19. A. Albu-Yaron, C. Levy-Clement, and J. L. Hutchison, *Electrochem. Solid-State Lett*., **2**, 627
305 (1999).
306 20. A. Albu-Yaron, C. Levy-Clement, A. Katty, S. Bastide, and R. Tenne, *Thin Solid Films*, **361-362**,
307 223 (2000).
308 21. S.K. Ghosh, T. Bera, O. Karacasu, A. Swarnakar, J.G. Buijnsters, and J.P. Celis, *Electrochim.*
309 *Acta*, **56**, 2433 (2011).
310 22. S. Shariza and T.J.S. Anand, *Chalcogen. Lett*., **8**, 529 (2011).
311 23. J. P. Nicholson, *J. Electrochem. Soc.*, **152**, C795 (2005).
312 24. Patrice Simon and Yury Gogotsi, *Nat. Mater*. **7**, 845 (2008).
313 25. Marta Sevilla and Robert Mokaya, *Energy Environ. Sci*. **7**, 1250 (2014).
314 26. B.E. Conway, *Electrochemical Supercapacitors: Scientific Fundamentals and Technological*
315 *Applications* (Springer Science and Business Media, New York, 2013).
316 27. J. Miller and B. Dunn, *Langmuir*, **15**, 799 (1999).
317 28. J.W. Long, K.E. Swider, C.I. Merzbacher, and D.R. Rolison, *Langmuir*, **15**, 780 (1999).
318 29. J. Miller, B. Dunn, T. Tran, and R Pekala, *J. Electrochem, Soc*,, **144**, L309 (1997).
319 30. B. Conway, V. Birss, and J. Wojtowicz, *J. Power Sources*, **66**, 1 (1997).
320 31. G.M. Swain, *J. Electrochem Soc.*, ***141***, 3382 (1994).
321 32. D. Merki, S. Fierro, H. Vrubel, and X.L. Hu, *Chem. Sci*., **2**, 1262 (2011).
322 33. J.F. You, D.X. Wu, and H.Q. Liu, *Polyhydron*, **5**, 535 (1986).
323 34. A.S. Goloveshkin, I.S. Bushmarinov, N.D. Lenenko, M.I. Buzin, A.S. Golub, and M. Yu.
324 Antipin, *J. Phys. Chem. C*, **117**, 8509 (2013).
325 35. A. N. Enyashin and A. L. Ivanovskii, *J. Struct. Chem*., **54**, 388 (2013).
326 36. T. Brousse, D. Belanger, and J.W. Long, *J. Electrochem. Soc.*, **162**, A5185 (2015).
327 37. C.C. Hu, K.H. Chang, M.C. Lin, and Y.T. Wu, *Nano Lett*., **6**, 2690 (2006).

328 38. Q. Lu, Z.J. Mellinger, W.G. Wang, W.F. Li, Y.P. Chen, J.G. Chen, and J.Q. Xiao,
329 *ChemSusChem*, **3**, 1367 (2011).
330 39. Z.Y. Lu, Q. Yang, W. Zhu, Z. Chang, J.F. Liu, X.M. Sun, D.G. Evans, and X. Duan, *Nano Res*.,
331 **5**, 369 (2012).
332 40. A. Ramadoss, T.H. Kim, G.S. Kim, and S.J. Kim, *New J. Chem*., **38**, 2379 (2014).
333 41. N. Choudhary, M. Patel, Y.H. Ho, N.B. Dahotre, W.K. Lee, J.Y. Hwang, and W.B. Choi, *J.*
334 *Mater. Chem. A*, **3**, 24029 (2015).
335 42. M.A. Bissett, I.A. Kinloch, and R.A. W. Dryfe, *ACS Appl. Mater. Interf*., **7**, 17388 (2015).
336 43. K. Gopalakrishnan, K. Pramoda, U. Maitra, U. Mahima, M. A. Shah, and C.N.R. Rao,
337 *Nanomater. Energy*, **4**, 9 (2015).
338 44. R. Thangappan, S. Kalaiselvam, A. Elayaperumal, R. Jayavel, M. Arivanandhan, R. Karthikey,
339 and Y. Hayakawa, *Dalton Trans*. **45**, 2637 (2016).
340 45. Meryl D. Stoller and Rodney S. Ruoff, *Energy Environ. Sci*., **3**, 1294 (2010).
341 46. K.J. Huang, L. Wang, J.Z. Zhang, L.L. Wang, and Y.P. Mo, *Energy*, **67**, 234 (2014).
342 47. H.M. Ji , C. Liu , T. Wang , J. Chen , Z.M. Mao , J. Zhao , W.H. Hou , and G. Yang, *Small*, **11**,
343 6480 (2015).
344 48. J.Y. Lei, Z.Q. Jiang, X.F. Lu, G.D. Nie, and C. Wang, *Electrochim. Acta*, **176**, 149 (2015).
345 49. J. Xu, L.J. Dong, C.S. Li, and H. Tang, *Mater. Lett*., **162**, 126 (2016).
346 50. J. Wanga, D.L. Chao, J.L. Liu, L.L. Li, L.F. Lai, J.Y. Lin, and Z.X. Shen, *Nano Energy*, **7**,151
347 (2014).
348 51. L.Q. Li, H.B. Yang, J. Yang, L.P. Zhang, J.W. Miao, Y.F. Zhang, C.C. Sun, W. Huang, X.C.
349 Dong, and B. Liu, *J. Mater. Chem. A*, **4**, 1319 (2016).
350
351
352
353
354

355 **Figure captions**

356 Figure 1. Cyclic voltammetry of a glassy carbon electrode (GCE) at 30 mV/sec with and without
357 10 mM $(NH_4)_2MoS_4$ in 0.2 M KCl at pH 6.8.

358 Figure 2. Top view (a) and cross-sectional (b) SEM images of 5 μm thick MoS_2 thin films atop
359 glassy carbon plate after annealing at 600°C in Ar for 1 h.

360 Figure 3. Powder x-ray diffraction of MoS_2 thin films scraped off glassy carbon plate after
361 annealing at 600°C in Ar for 1 h.

362 Figure 4. Cyclic voltammetry curves at different scan rates in 1.0 M Na_2SO_4 for 1 μm as-deposited
363 film (a); and 50 nm (b), 1 μm (c) and 5 μm (d) annealed MoS_2 thin film atop glassy
364 carbon plate.

365 Figure 5. Capacitance measurements from cyclic voltammetry at 10 mV/s scan rate for different
366 thickness of annealed MoS_2 thin films in units of F/g (a) and F/cm^2 (b) during 1000
367 cycles in 1.0 M Na_2SO_4.

368 Figure 6. Specific capacitance measured for first cycle as a function of scan rate and film thickness
369 for annealed MoS_2 films.

370 Figure 7. Galvanostatic charge/discharge curves of 50 nm (a), 1μm (b) and 5 μm (c) annealed
371 MoS_2 films at different charge/discharge current densities.

372 Figure 8. Effect of charge/discharge current density on the specific capacitance obtained for
373 different MoS_2 film thickness.

374 Figure 9. Capacitance measurements from galvanostatic charge/discharge technique for different
375 thickness of MoS_2 thin films during 1000 cycles in 1.0 M Na_2SO_4.

376 Figure 10. Nyquist plot of EIS results in 1.0 M Na_2SO_4 for MoS_2 film atop glassy carbon plate,
377 before and after capacitance testing.

378

379

380

381

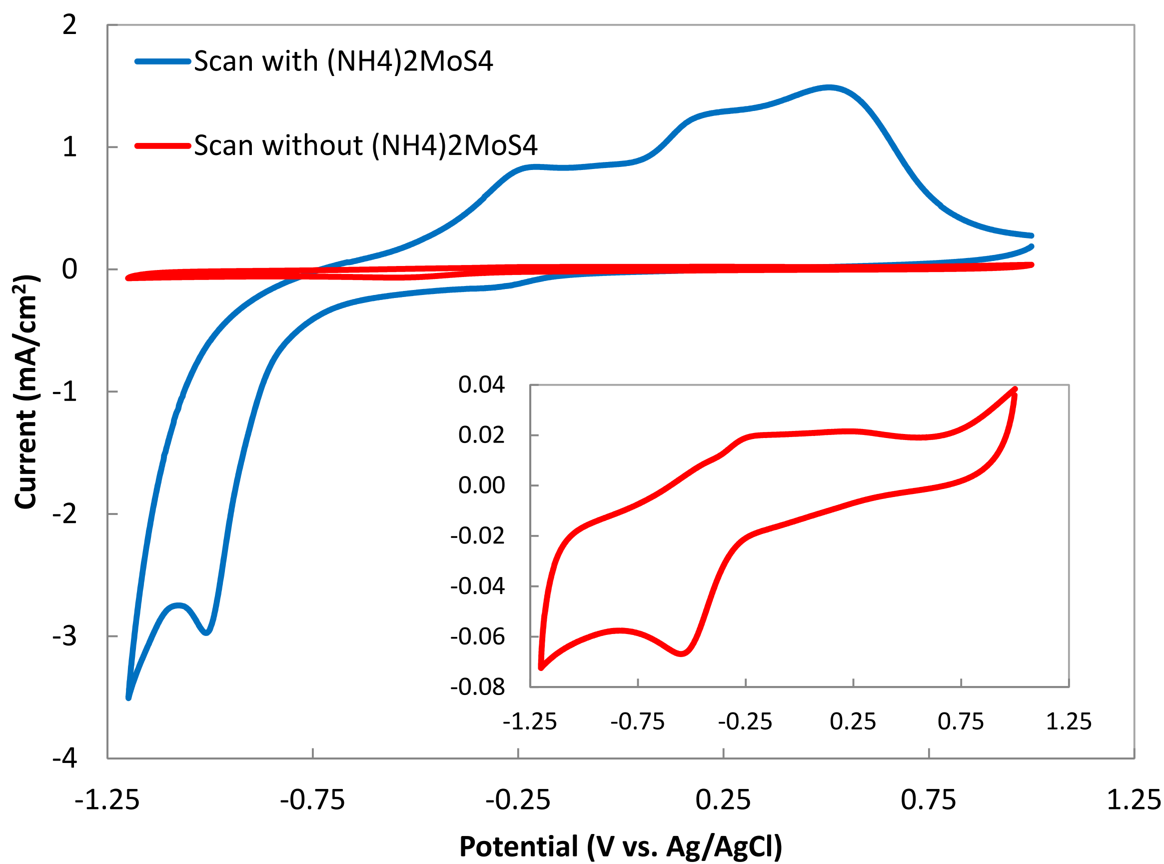

382

383

384 Figure 1.

385

386

387

388

389

390

391

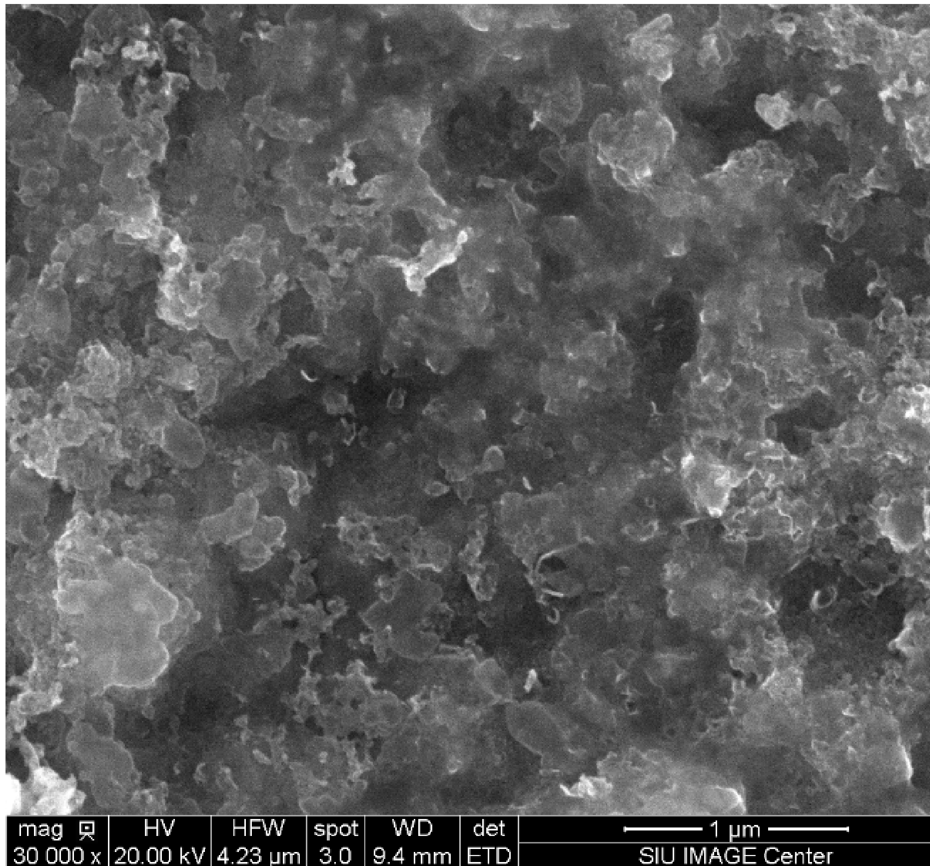

392

393

394

395

396 Figure 2a.

397

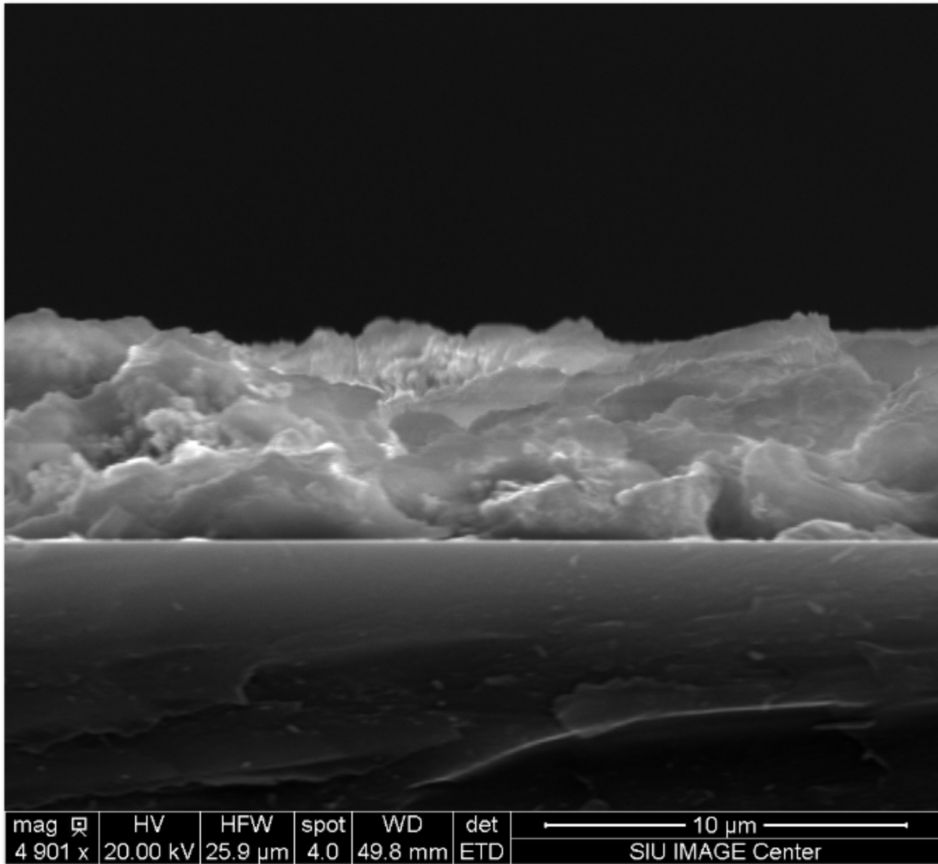

398

399 Figure 2b.

400

401

402

403

404

405

406

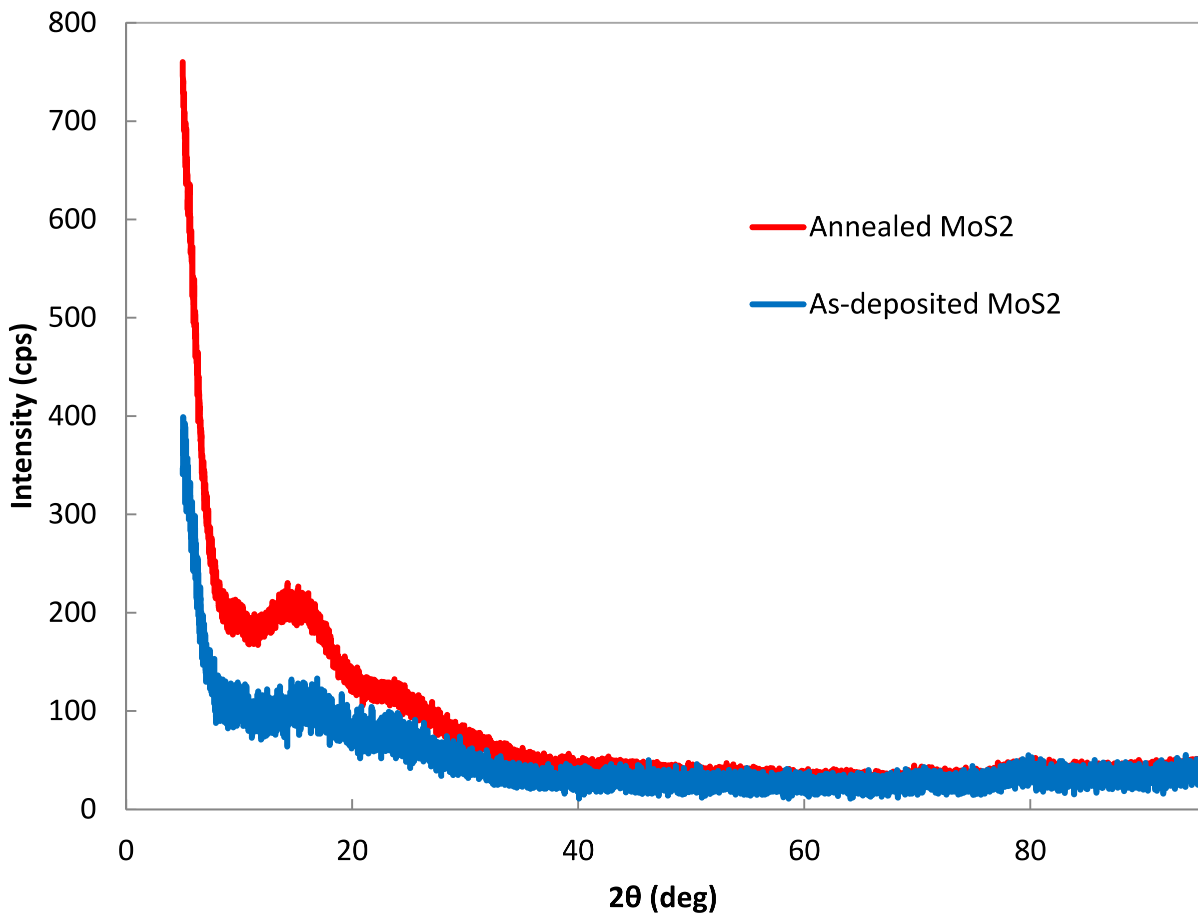

407

408

409 Figure 3.

410

411

412

413

414

415

416

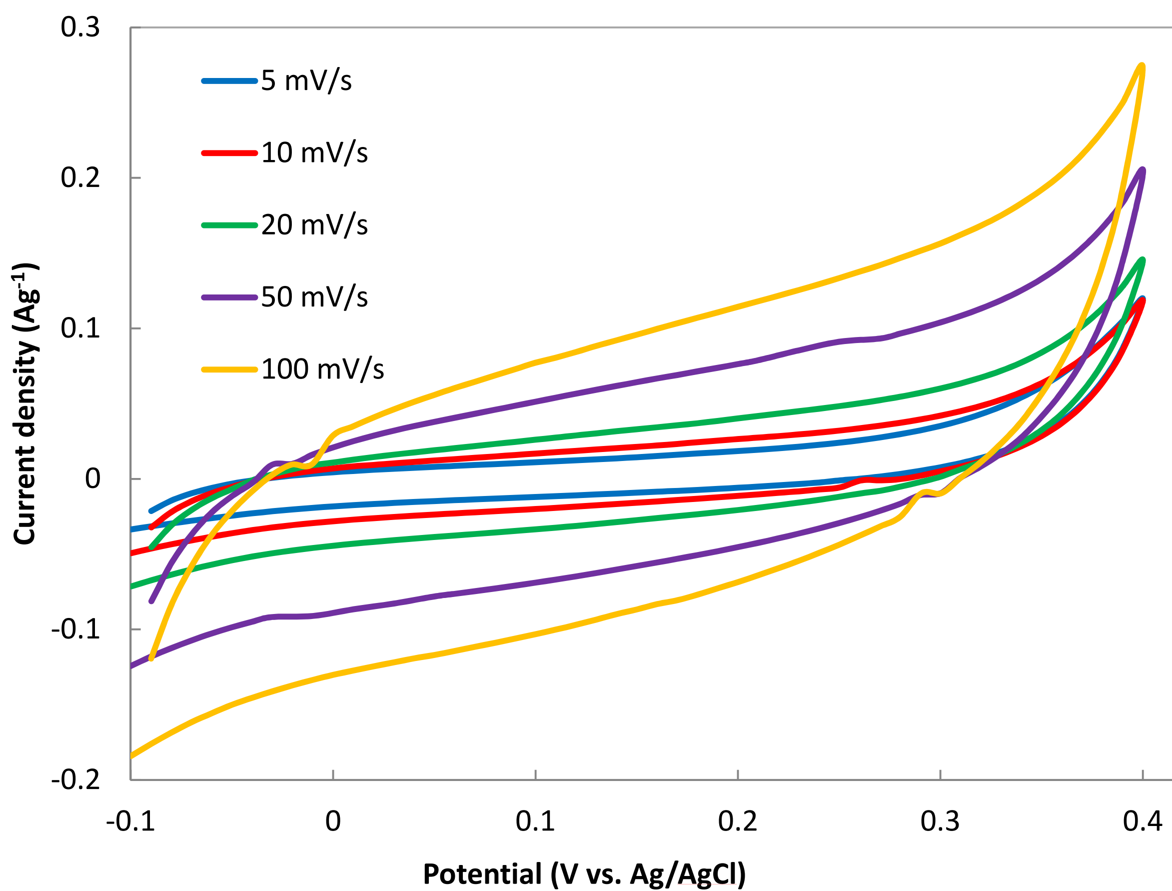

417

418

419 Figure 4a.

420

421

422

423

424

425

426

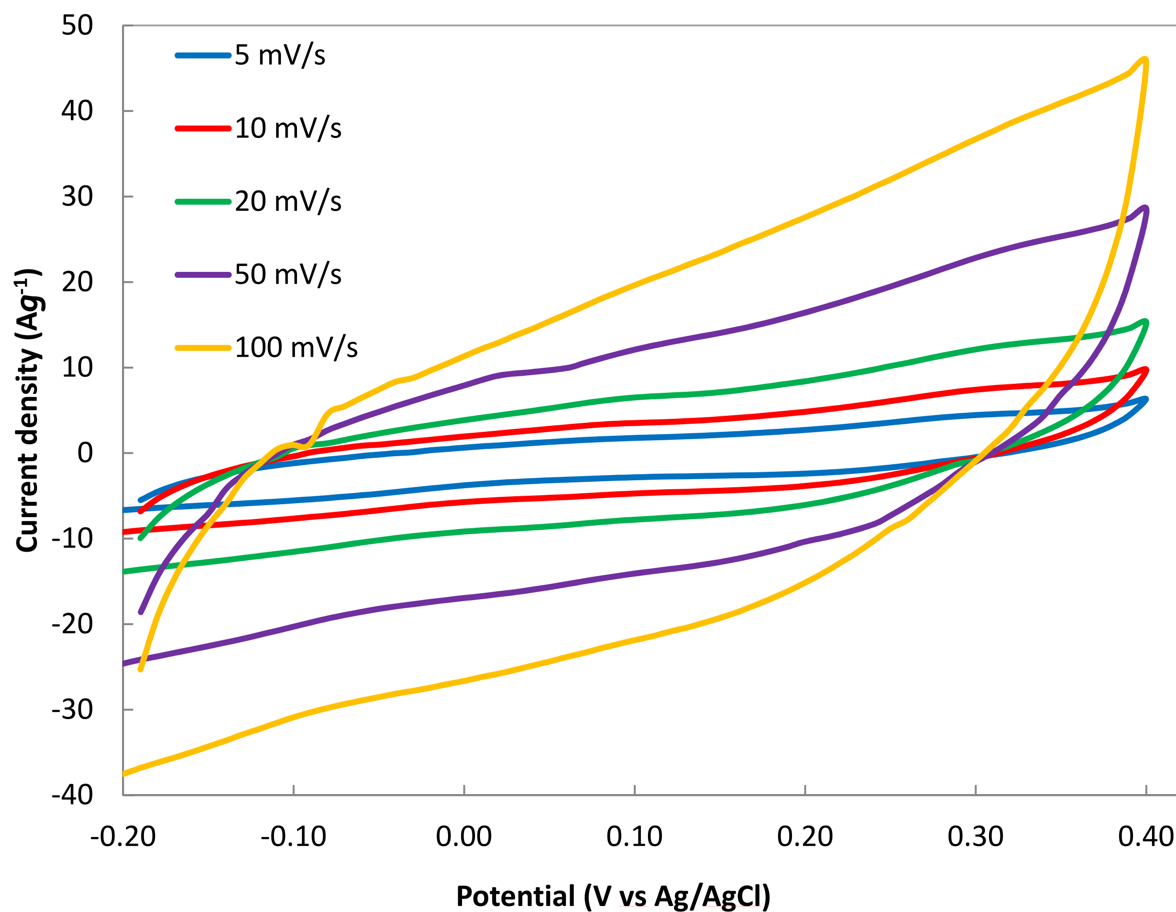

427

428 Figure 4b.

429

430

431

432

433

434

435

436

437

438

439

440

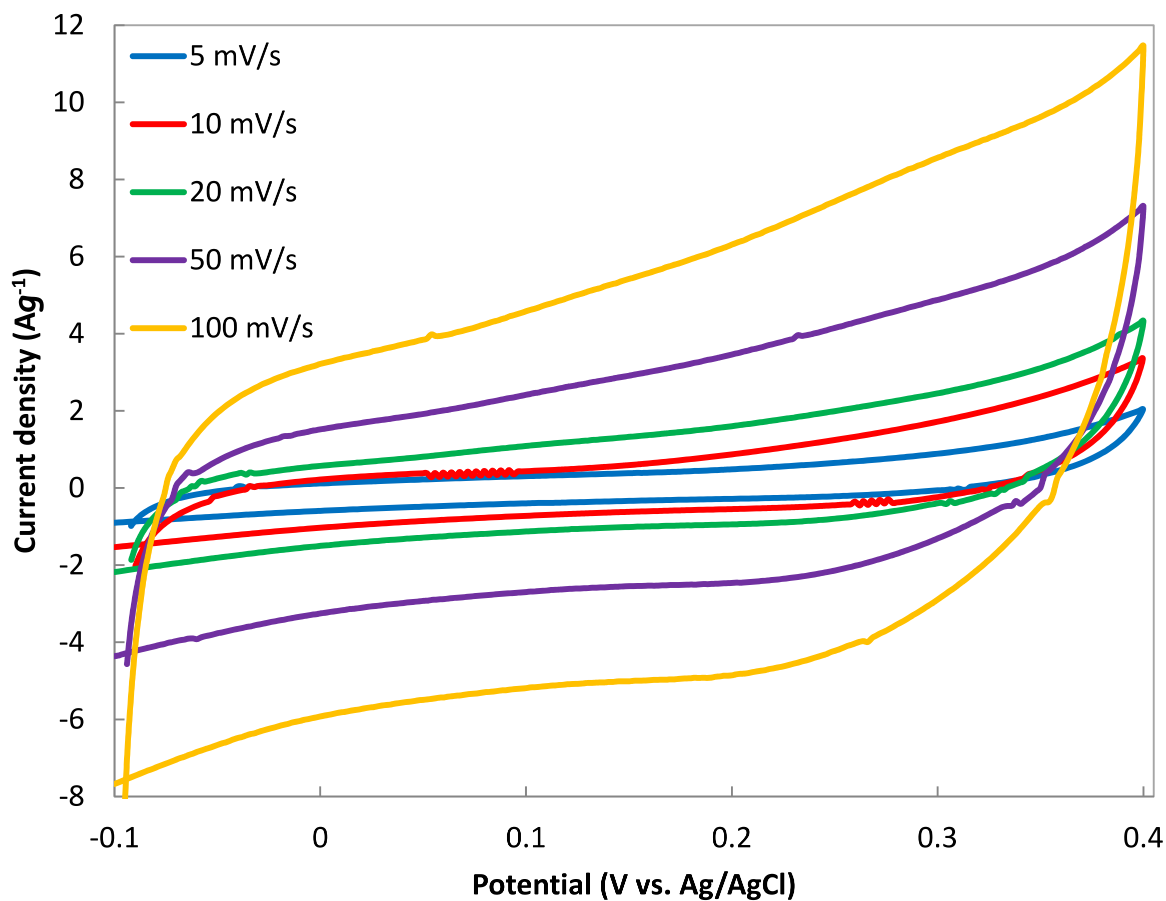

441

442 Figure 4c.

443

444

445

446

447

448

449

450

451

452

453

454

455

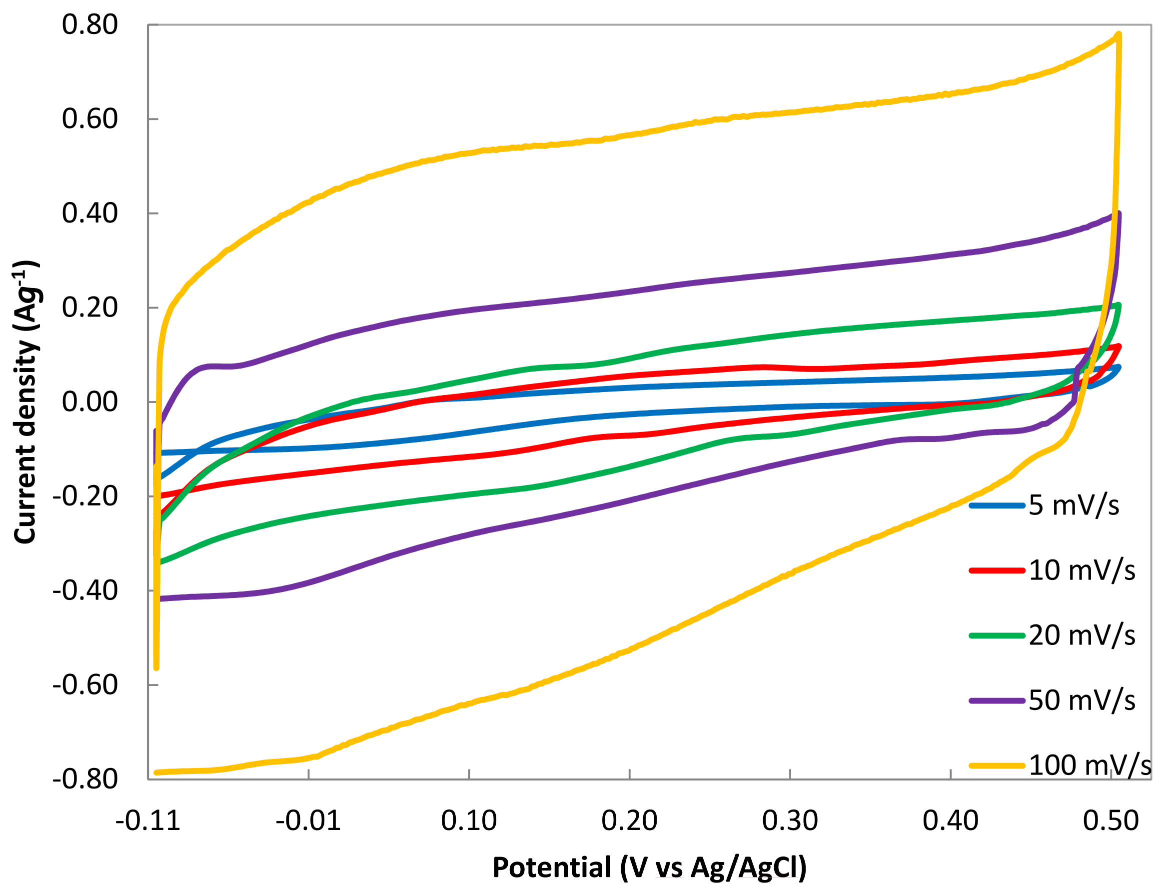

456

457 Figure 4d.

458

459

460

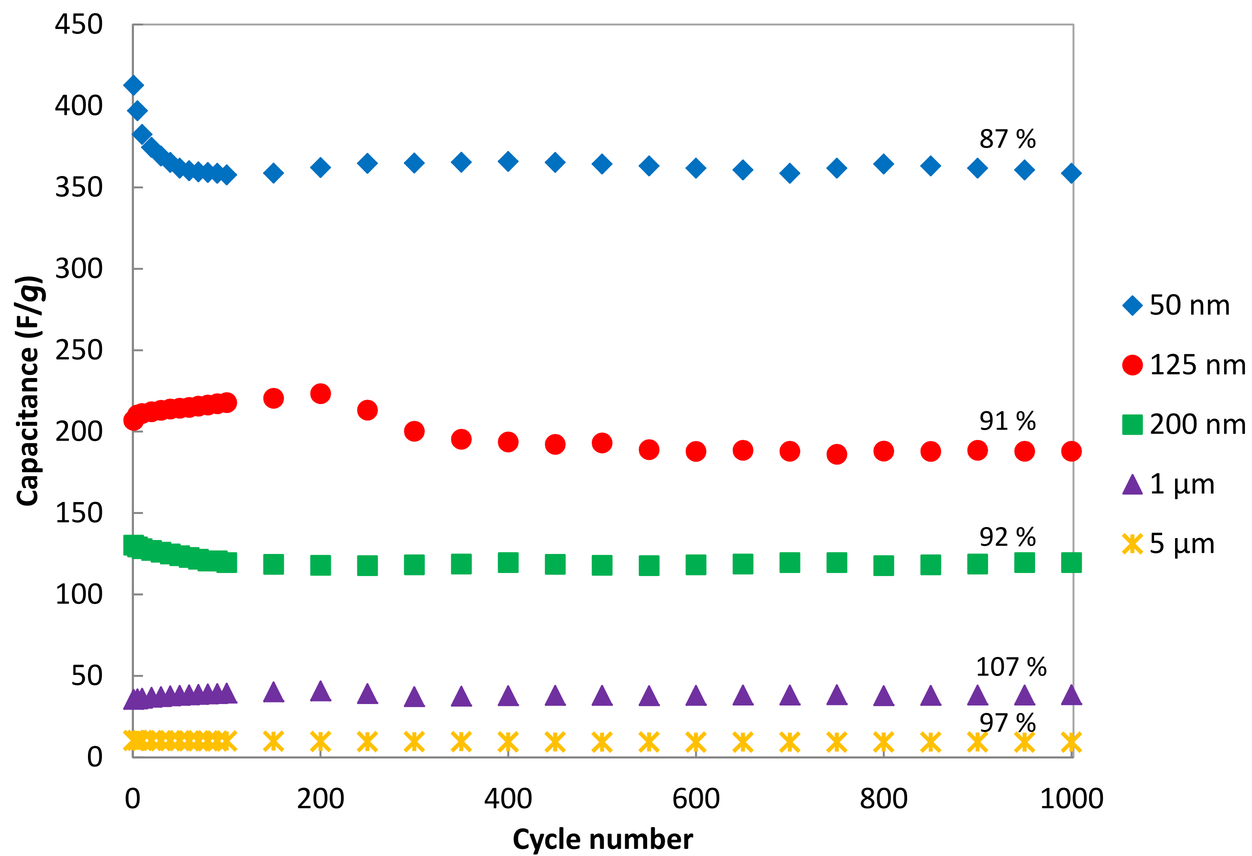

461

462 Figure 5a.

463

464

465

466

467

468

469

470

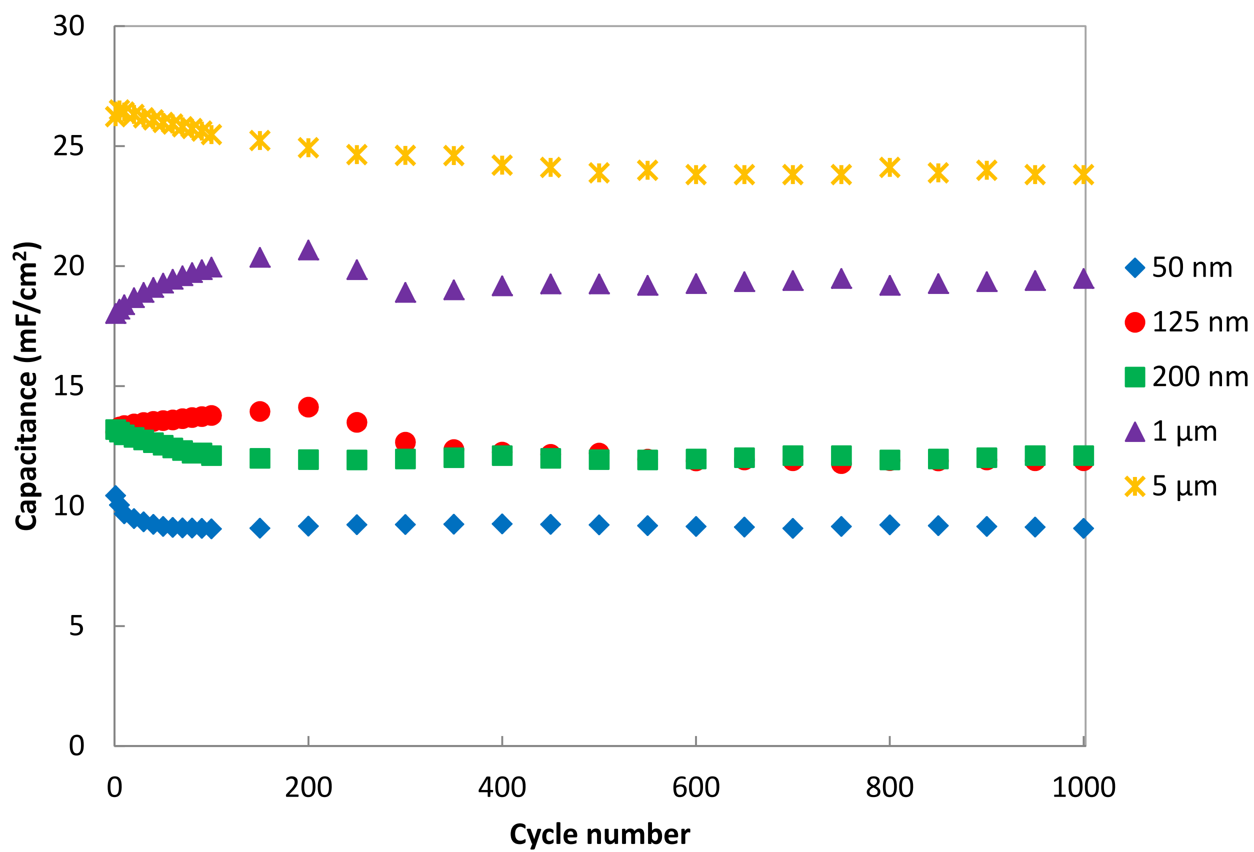

471

472

473 Figure 5b.

474

475

476

477

478

479

480

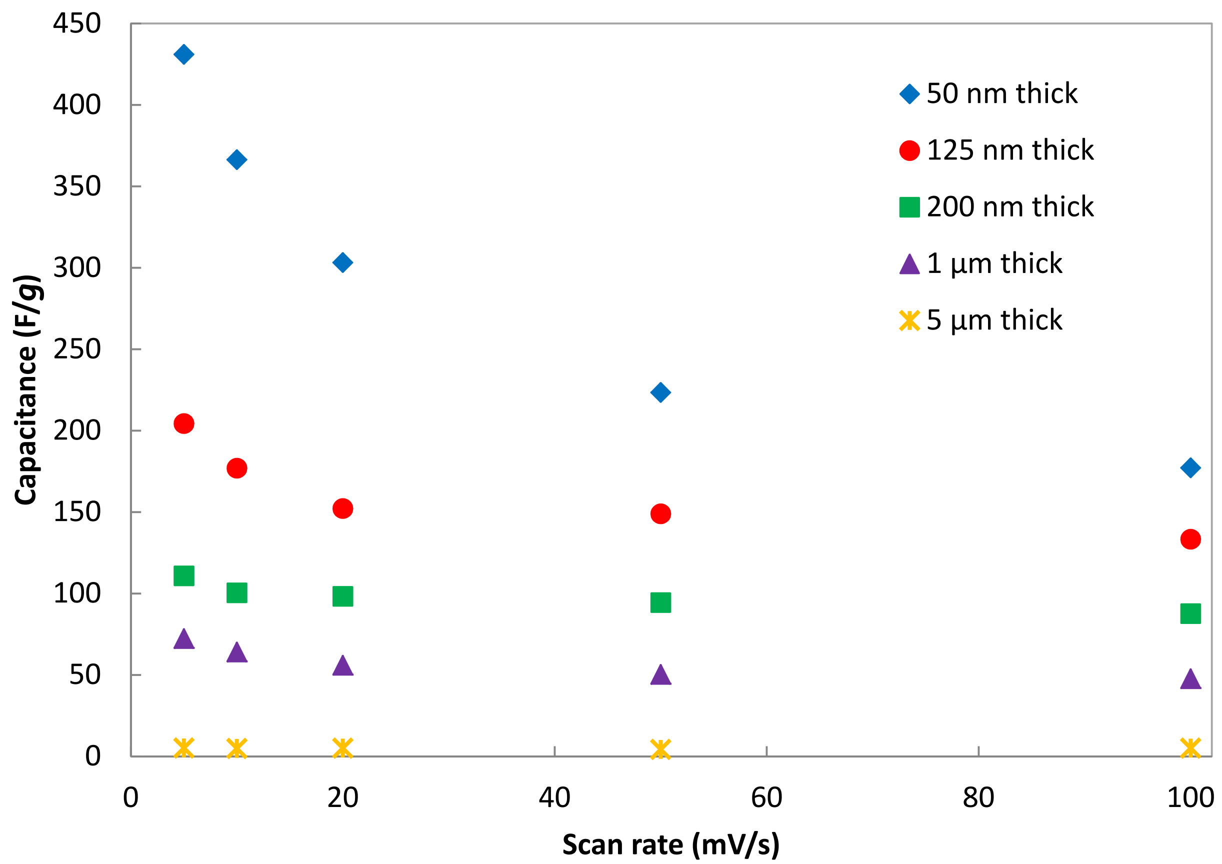

481

482

483 Figure 6.

484

485

486

487

488

489

490

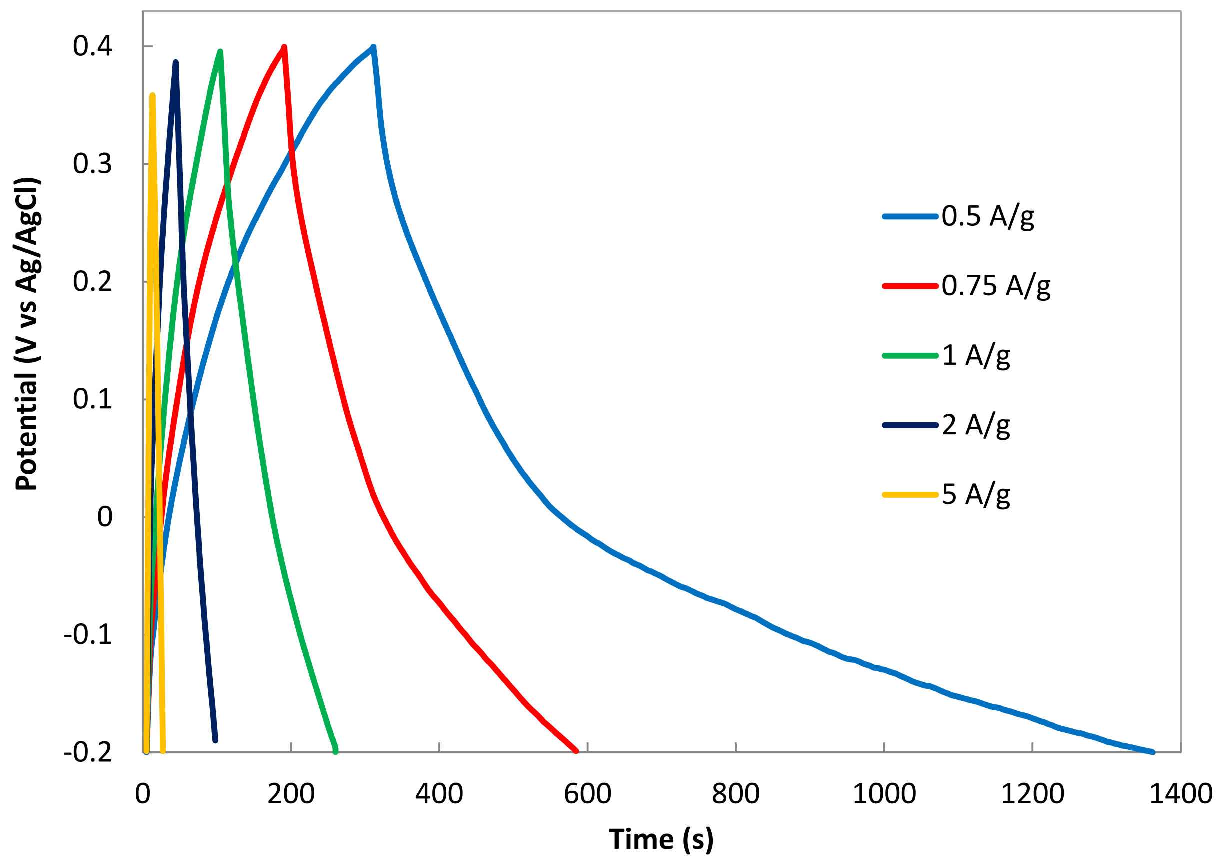

491

492 Figure 7a.

493

494

495

496

497

498

499

500

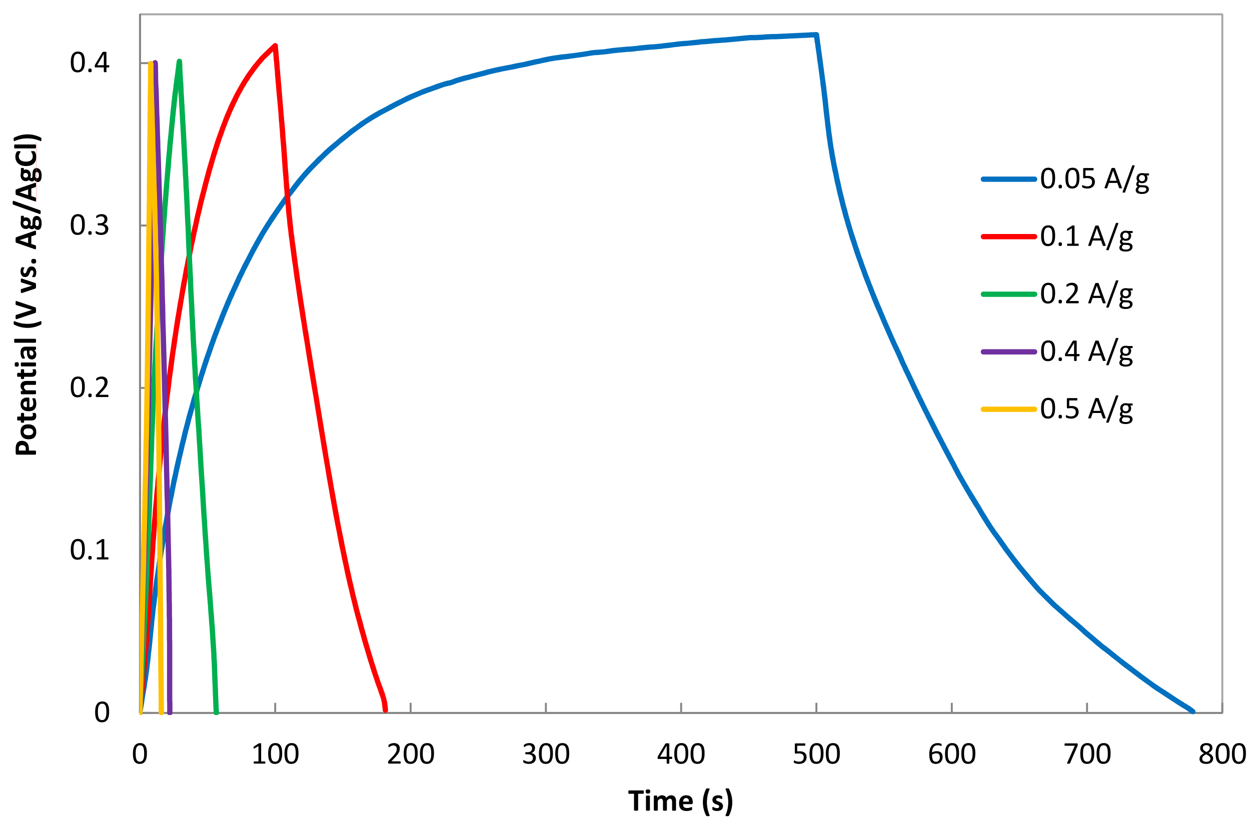

501

502 Figure 7b

503

504

505

506

507

508

509

510

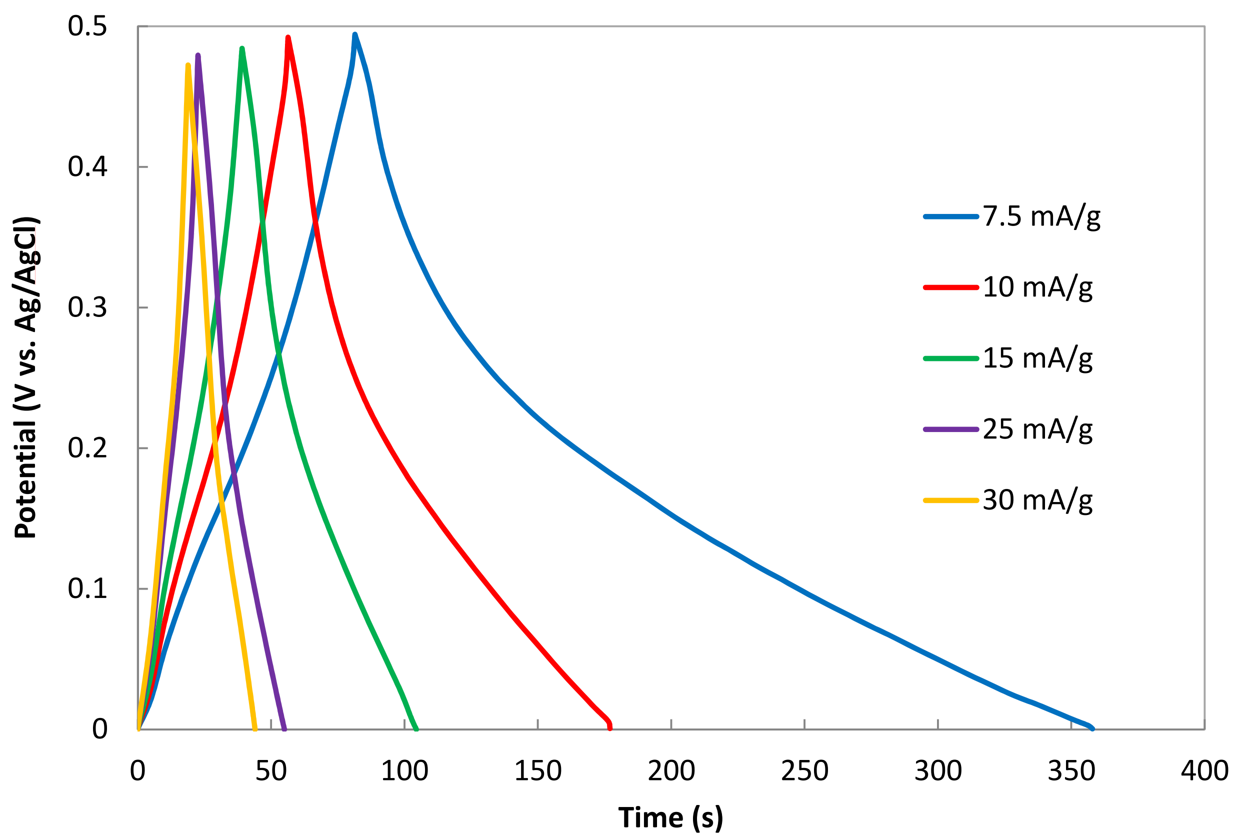

511

512 Figure 7c

513

514

515

516

517

518

519

520

521

522

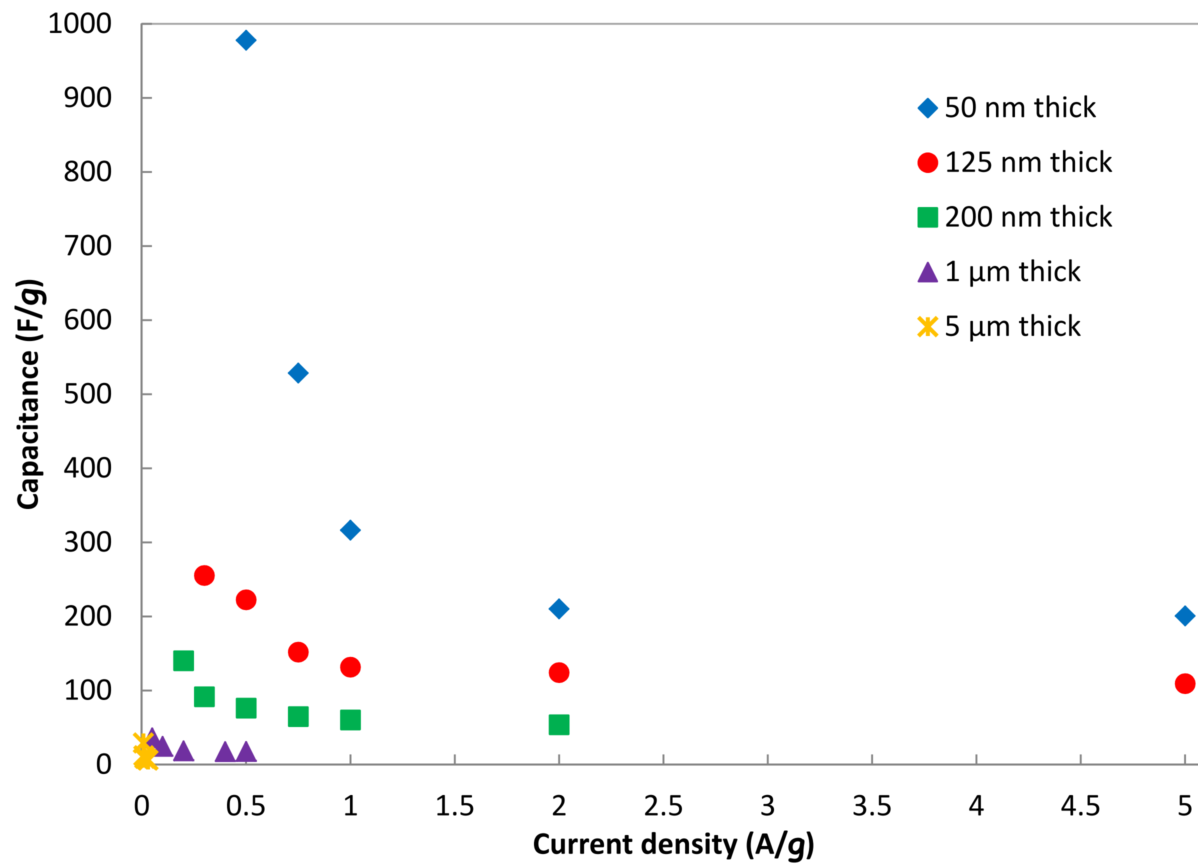

523

524

525

526 Figure 8.

527

528

529

530

531

532

533

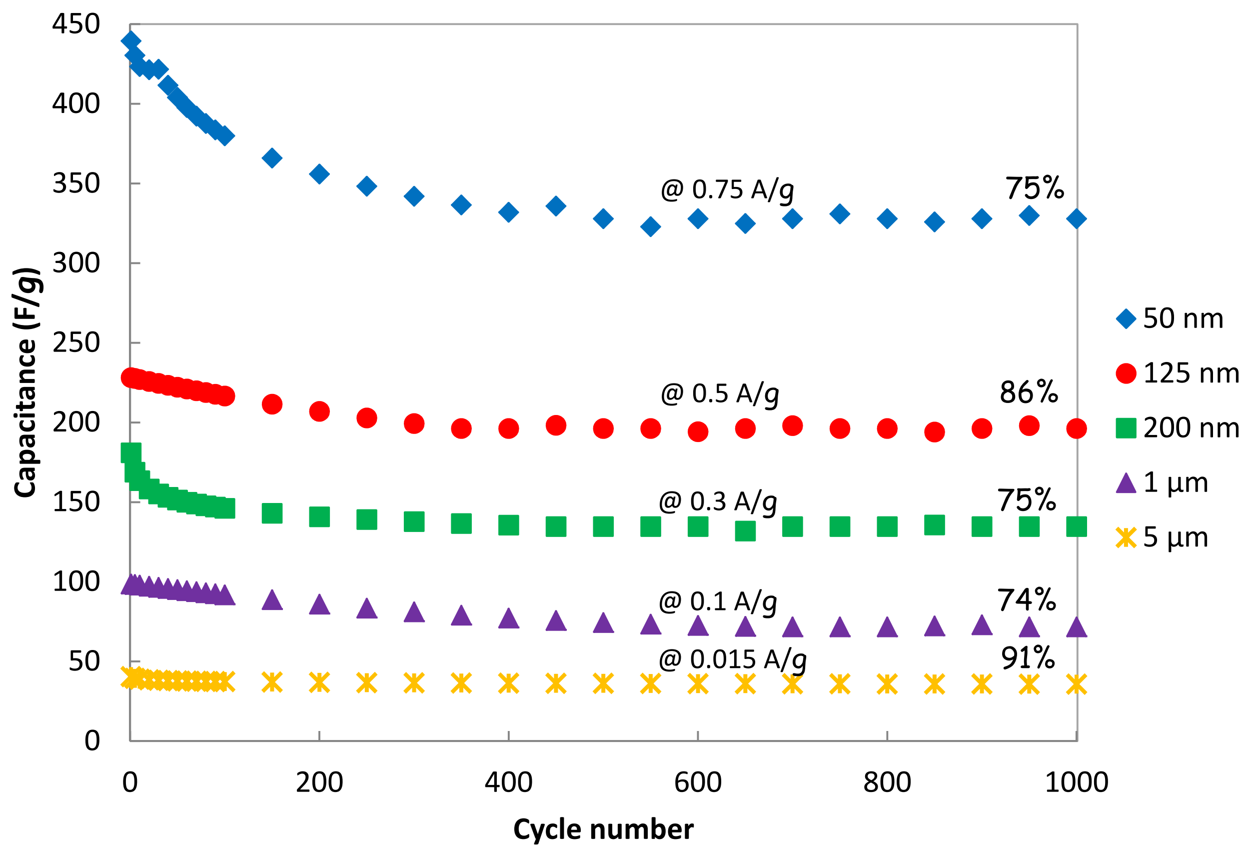

534

535

536 Figure 9.

537

538

539

540

541

542

543

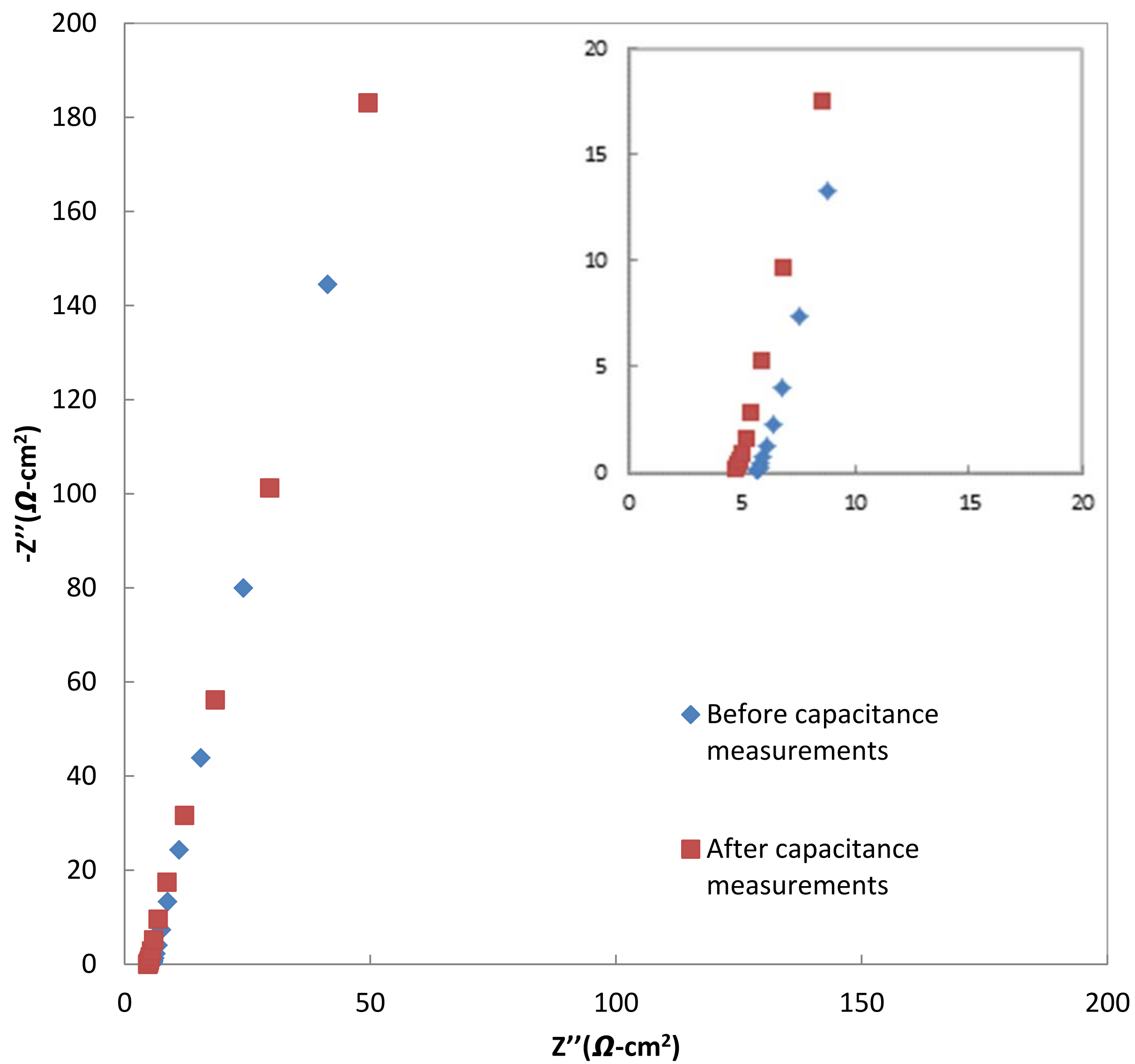

544

545

546 Figure 10.

547

548